Journal of the Ceramic Society of Japan 127 [1] 28-34 2019
DOI http://doi.org/10.2109/jcersj2.18146

JCS-Japan

FULL PAPER

Development of liquid scintillators loaded with alkaline earth molybdate nanoparticles for detection of neutrinoless double-beta decay

Sae ARAI[1,†], Takio NOGUCHI[2], Tsutomu AIDA[2], Akira YOKO[3], Takaaki TOMAI[4], Tadafumi ADSCHIRI[3], Masanori KOSHIMIZU[1], Yutaka FUJIMOTO[1] and Keisuke ASAI[1]

[1] Department of Applied Chemistry, Graduate School of Engineering, Tohoku University, 6–6–07 Aoba, Aramaki, Aoba-ku, Sendai 980–8579, Japan
[2] New Industry Creation Hatchery Center, Tohoku University, 6–6–10 Aoba, Aramaki, Aoba-ku, Sendai 980–8579, Japan
[3] WPI Advanced Institute for Materials Research, Tohoku University, 2–1–1 Katahira, Aoba-ku, Sendai 980–8577, Japan
[4] Institute of Multidisciplinary Research for Advanced Materials, Tohoku University, 2–1–1 Katahira, Aoba-ku, Sendai 980–8577, Japan

To determine whether neutrinoless double-beta decay occurs is an enormous challenge in particle physics. For this purpose, developing a highly transparent liquid scintillator that contains a candidate isotope at high concentration is required. In this work, ^{100}Mo was selected as the isotope and surface-modified nanoparticles were applied. $AMoO_4$ alkaline earth molybdates (A = Ca, Sr, and Ba) were synthesized with a subcritical hydrothermal method so that they were well dispersed in organic solvents. The crystalline phase of the nanoparticles was confirmed with X-ray diffraction measurements. The particle size of $SrMoO_4$ nanoparticles was found to be the smallest from a transmission electron microscope examination. The $SrMoO_4$ nanoparticles were incorporated in liquid scintillators, resulting in high transparency and efficient scintillation. In conclusion, liquid scintillators loaded with organic modified $SrMoO_4$ nanoparticles were successfully developed.

Key-words : Neutrinoless double-beta decay, Liquid scintillator, Alkaline earth molybdate, Hydrotherrmal synthesis

[Received July 31, 2018; Accepted November 2, 2018]

1. Introduction

Neutrinoless double-beta decay is a process of double-beta decay without the emission of a neutrino. The confirmation of its presence or absence is important in current particle physics.[1),2)] Double-beta decay is a type of radioactive event where two protons transform into two neutrons and two beta-rays. The process has been observed for some radioactive nuclides. However, the presence of neutrinoless double-beta decay has not been confirmed. If its presence is confirmed, it will affirms that a neutrino has a finite mass and an anti-neutrino is the same as a neutrino itself. Detection of neutrinoless double-beta decay is difficult because the estimated half-life for the decay mode is long, typically 10^{22} years.[1),2)] In detectors containing large quantities of a candidate isotope, around 3.0 wt %[3)] concentration is necessary to accumulate sufficient detection events to provide statistical confirmation in a reasonable time period. Neutrinoless double-beta decay can be distinguished from double-beta decay with neutrino emission on the basis of the difference in the total energies of the two beta-rays. Hence, a detector with high energy resolution is necessary. Various types of detector systems have been proposed to fulfill the criteria of large quantities of the candidate isotope and high energy resolution[3)–5)]

Liquid scintillators loaded with a candidate isotope is one such type of detector systems. In detectors systems in which a candidate isotope and the detector are separated, some of the beta-rays from the isotopes are back-scattered at the window of the detector and thus not detected. In contrast, in the case of liquid scintillators, the candidate isotope is included in the detector and thus can be detected without loss. In addition, liquid scintillators generally have a sufficient energy resolution.

Several research groups have developed such liquid scintillators by dissolving organometallic molecules or salts comprising a candidate isotope into liquid scintillators.[6)–8)] However, this approach has problems because the typical value of the candidate isotope concentration in liquid scintillators is limited on the order of 0.1 wt %, and quenching is caused by quenchers and phosphors, result-

† Corresponding author: S. Arai; E-mail: key13.aray.pp@gmail.com

Table 1. Amounts of solvent and $CaMoO_4$ sources, modifiers and yields

PHA:OAm	$CaMoO_4$ source [mmol]		the amount of solvent [mL]	Modifier [mmol]		Yield [%]	Mo ion to the modifier molecules [mol:mol]
	$MoO_2(acac)_2$	$Ca(acac)_2$		PHA	OAm		
1:0	0.375	0.375	3.75	0.750	0.00	15.5	1:2
1:1	0.375	0.375	3.75	0.750	0.750	21.4	1:4
1:2	0.375	0.375	3.75	1.50	1.50	30.5	1:8
2:1	0.375	0.375	3.75	1.50	0.750	20.4	1:6
0:1	0.375	0.375	3.75	0.00	0.750	12.3	1:2

ing in a low scintillation efficiency and insufficient energy resolution.

To solve these problems, we propose the method of loading nanoparticles containing a candidate isotope in a liquid scintillator. To increase the dispersion concentration in organic solvents used for liquid scintillators, organically modified nanoparticles are appropriate because they readily disperse in organic solvents at high concentrations. Super- and subcritical hydrothermal methods[9)–12)] are suitable to synthesize such nanoparticles. Our group succeeded in developing liquid scintillators loaded with ZrO_2 nanoparticles, comprising ^{96}Zr candidate isotope using the hydrothermal methods. The loading amount of ^{96}Zr in the ZrO_2 nanoparticles dispersion reached 1.4 wt %, which is significantly higher than that of previous studies.[13)]

In this study, another candidate isotope, ^{100}Mo, was focused on for neutrinoless double-beta decay because ^{100}Mo is present in abundant in nature, and it is less subject to background noise owing to the large Q-value in double beta-decay. Among candidate compounds to form nanocrystals, those that have crystal structures comprising tetrahedrally-coordinated Mo^{6+} is chosen because of their high optical transition energy, which results in optical transparency in the visible region. In addition, when doped with rare-earth ions, the crystals exhibit high luminescence quantum efficiency owing to the efficient energy transfer from Mo^{6+} to rare earth ions.[14)]

$AMoO_4$ (A = Ca, Sr, and Ba) nanoparticles comprising Mo^{6+} was synthesized to be dispersed in liquid scintillators. In this paper, the synthesis and characterization of the $AMoO_4$ nanoparticles are described. To achieve a high dispersion concentration in liquid scintillators, organically modified $AMoO_4$ nanoparticles were synthesized using the hydrothermal method. In the field of solid catalysts, it is discussed that the degree of acidity or base differs depending on kinds of oxide.[15)] In this study, therefore, we synthesized $AMoO_4$ nanoparticles by changing the ratios of carboxylic acid and amine as modifiers.

Finally, liquid scintillators containing the smallest and high dispersion concentration nanoparticles among the synthesized $AMoO_4$ nanoparticles were fabricated and evaluated. The nanoparticles were dispersed in toluene, which is in common use as a liquid scintillator solvent. The optical transparencies and the scintillation properties of the nanoparticle dispersions are also presented.

2. Experimental procedures

$AMoO_4$ nanoparticles were synthesized with subcritical hydrothermal methods in batch reactors made of Hastelloy C, which is a nickel-based alloy with high resistance to corrosion at high temperatures. The batch reactor had an inner volume of 5 mL. $MoO_2(acac)_2$ (Wako) was first dissolved in distilled water at a concentration of 0.1 mol/L, and $A(acac)_2$ (Aldrich) was added to the solution. This precursor solution of 3.75 mL was loaded into the reactors. As the organically modifying materials, 6-phenylhexanoic acid (PHA; Tokyo Chemical Industry) and octylamine (OAm; Tokyo Chemical Industry) were added to the precursor solutions. The molar ratio of PHA to OAm was changed as shown in **Table 1**. Reactions were carried out under 300°C and 30 MPa for 10 min with shaking, followed by the quenching of the reactors with water bath at room temperature. After the liquid and solid products were collected, the reactor was rinsed several times with 3.75 mL of toluene and 3.75 mL of ethanol (99.5%; Wako). The rinsing solutions were mixed with the recovered products to extract the organically modified $AMoO_4$ nanoparticles into the toluene phase. The organic and water phases of the mixture were separated by making the mixture stand overnight. Subsequently, the organic phase was used as the nanoparticle dispersion in 10 mL of toluene. To obtain the nanoparticles in powder form, 10 mL of ethanol (99.5%, Wako) was added to the nanoparticle-toluene dispersion to dissolve extra modifier, and subsequently the dispersion was centrifuged, and the supernatant in the dispersion was removed. This procedure was repeated three times. Subsequently, the remaining precipitation was dried on a Petri dish under 60°C. The yields of $AMoO_4$ nanoparticles were shown in Tables 1 and **2**.

Table 2. Yields of $AMoO_4$ synthesized with PHA:OAm = 1:2

A	the amount of solvent [mL]	Yield [%]
Ca	3.75	30.5
Ba	3.75	27.1
Sr	3.75	25.8

To determine the crystalline phase of the nanoparticles, the dried powder was analyzed with X-ray diffraction (XRD) measurements (Ultima IV, Rigaku) using Cu Kα radiation in a 2θ-θ setup; the scan interval and rate were 0.02° and 1.0 degree/min, respectively. The shapes and particle sizes of the nanoparticles were observed with a transmission electron microscope (TEM; HD-2700, Hitachi High-Technologies) operated at 200 kV. A drop of the nanoparticle dispersions in toluene was dried on copper grids (NP-C15, Okenshoji) and then TEM observation was conducted. The nanoparticle diameters were obtained as an average of 50 particles. Thermal properties of nanoparticle

powders were measured with a thermogravimetric analyzer (TGA; SDT Q600, TA Instruments Japan Inc.) using a heating rate of 20 °C/min up to 500°C in an air atmosphere. The ratios of PHA:OAm on surface of produced nanoparticles were calculated by organic trace element analyzer (CHNS; Elementar, vario EL cube). After dissolving the nanoparticles into 15% hydrochloric acid, inductively coupled plasma atomic emission spectroscopy (ICP-AES) analyses were performed (iCAP6500, Thermo Fisher) at an emission wavelength of 202 nm to determine the Mo concentrations in the toluene nanoparticle dispersions. The absorption spectra of the toluene dispersions were acquired with a spectrophotometer (U3500, Hitachi), using a quartz cell with a 1-cm optical path length. X-ray photoelectron spectroscopy (XPS; AXIS-ULTRA), using Al Kα radiation with 20 meV pass energy and 100.0 meV energy step, was performed for powder samples to confirm the valence state of Mo in the synthesized samples.

Liquid scintillators were fabricated using the toluene dispersions of nanoparticles with $SrMoO_4$ nanoparticles. As luminescent materials, 2,5-diphenyloxazole (DPO; Dojindo) and 1,4-bis(5-phenyl-2-oxazolyl) benzene (POPOP; Dojindo) were added to the toluene dispersion. At first, DPO and POPOP were mixed homogeneously in a weight ratio of 80:1, and then the mixture was subsequently added to the toluene dispersion of nanoparticles. The X-ray-induced radioluminescence spectra of the liquid scintillators incorporating the $AMoO_4$ nanoparticles were acquired. Each liquid scintillator was placed in a quartz cell and irradiated with X-rays from an X-ray generator (D2300-HK, Rigaku) equipped with a Cu target operating at 40 kV and 40 mA, and the resulting scintillations were detected with an optical multichannel analyzer (MCPD-3000, Otsuka Electronics) via an optical fiber.

3. Results and discussion

Figure 1 shows the XRD patterns of the $CaMoO_4$ nanoparticles synthesized with different molar ratios of PHA and OAm. The XRD patterns of nanoparticles were attributed to scheelite tetragonal $CaMoO_4$ ($I4_1/a$, S.G. 88);

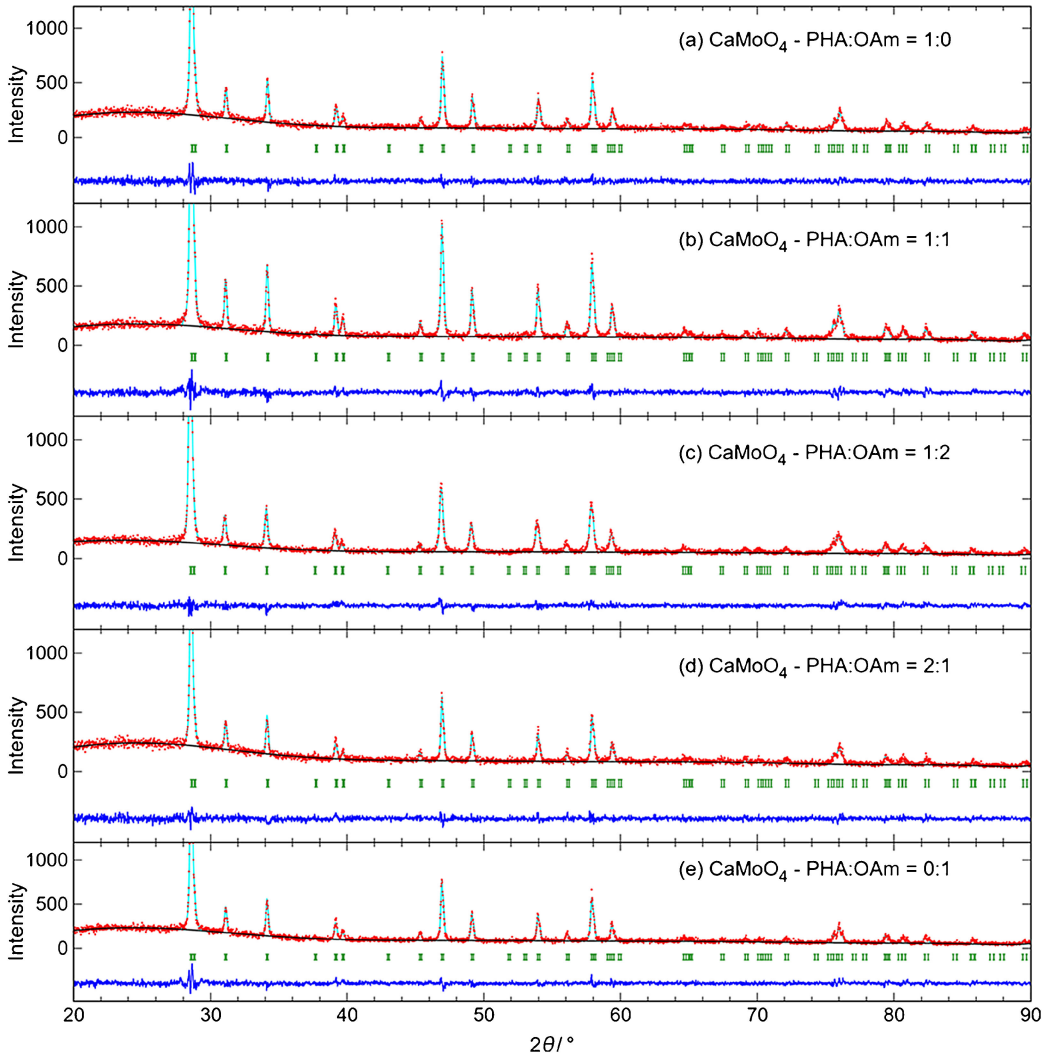

Fig. 1. XRD patterns of $CaMoO_4$ nanoparticles synthesized in different molar ratios of PHA and OAm. (a) PHA:OAm = 1:0, (b) PHA:Oam = 1:1, (c) PHA:Oam = 1:2, (d) PHA:OAm = 2:1, and (e) PHA:OAm = 0:1. Rietveld analysis was conducted and the fittings were well converged as (a) $R_{wp} = 11.64$, $S = 1.38$; (b) $R_{wp} = 12.55$, $S = 1.45$; (c) $R_{wp} = 13.52$, $S = 1.39$; (d) $R_{wp} = 11.66$, $S = 1.37$; and (e) $R_{wp} = 12.27$, $S = 1.44$.

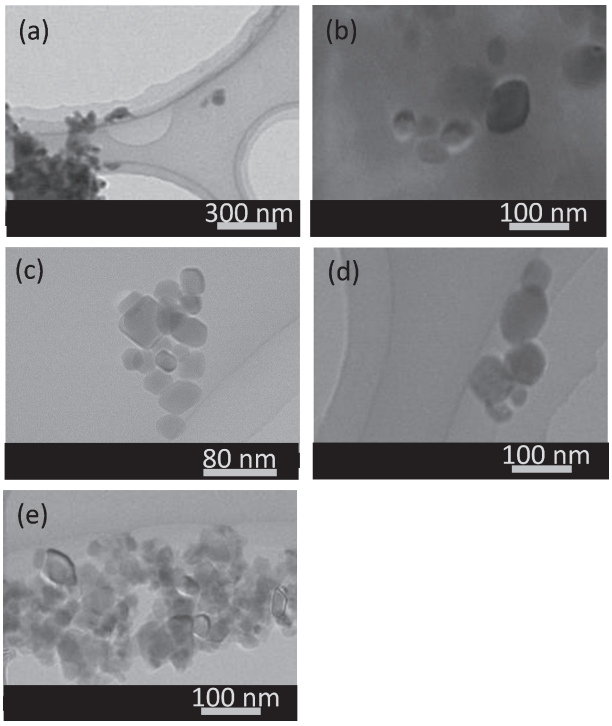

Fig. 2. TEM images of $CaMoO_4$ nanoparticles synthesized in different molar ratios of PHA and OAm. (a) PHA:OAm = 1:0, (b) PHA:OAm = 1:1, (c) PHA:OAm = 1:2, (d) PHA:OAm = 2:1, and (e) PHA:OAm = 0:1.

no other phase was observed. The broad diffraction peaks in the XRD patterns indicate small crystallite sizes.

The crystallite size was calculated by Halder-Wagner method[16] via Rietveld fittings with the RIETAN-FP[17] code. Halder-Wagner equation can be written as follows:

$$\left(\frac{\beta}{\tan\theta}\right)^2 = \frac{K\lambda}{D} \times \frac{\beta}{\tan\theta\sin\theta} + 16\varepsilon^2 \qquad (1)$$

Here, β is integral breadth (in radians), θ is Bragg angle, K is a constant (= 4/3 for the mean volume-weighted size of spherical crystallites[18]), λ (= 0.15418 nm) is the wavelength of the Cu Kα X-ray, D is the crystallite size, and ε is micro strain of the crystal. Crystallite size was 52 nm for (a) PHA:OAm = 1:0, 52 nm for (b) PHA:OAm = 1:1, 40 nm for (c) PHA:OAm = 1:2, 51 nm for (d) PHA:OAm = 2:1, and 53 nm for (e) PHA:OAm = 0:1. A very small crystallite was observed in sample (c) PHA:OAm = 1:2, suggesting that a higher density of modification occurred under the condition.

Figure 2 shows the TEM images of the $CaMoO_4$ nanoparticles. The diameters of the nanoparticles synthesized in molar ratios of PHA:OAm = 1:0, 1:1, 1:2, 2:1, and 0:1 are 58 ± 12, 49 ± 21, 33 ± 6, 53 ± 23, and 39 ± 5 nm, respectively. The tendency of the particle size change observed from TEM was consistent with that from XRD. The particle size of the $CaMoO_4$ nanoparticle was the smallest under the condition of PHA:OAm = 1:2. The effect of pH is not a main factor that determines the particle size because the pH of different nanoparticle dispersions was not significantly different before and after these synthesis processes. It has been reported that the diameter of the nanoparticle formed at high amine concentration was smaller because of the modification by oleic acid and oleylamine. The small diameter has been attributed to the sufficient coverage of the surface of nanoparticles to suppress their aggregations[19] and the interactions between amine and acid.[20] High density modification of the surface of the nanoparticles suppresses the growth and aggregation of the nanoparticles. The smallest nanoparticles were obtained with PHA:OAm = 1:2, possibly because of the same reason. Therefore, $AMoO_4$ nanoparticles were synthesized with PHA:OAm = 1:2.

Figure 3 shows the XRD patterns of $AMoO_4$ nanoparticles synthesized with PHA:OAm = 1:2. The crystallite size was 40 nm for (a) $CaMoO_4$, 62 nm for (b) $BaMoO_4$, and 51 nm for (c) $SrMoO_4$.

The observed patterns indicate that all the products have a scheelite tetragonal structure ($I4_1/a$, S.G. 88). The XRD patterns of the nanoparticles are attributable to the peaks of $CaMoO_4$, $BaMoO_4$, and $SrMoO_4$.

Figure 4 shows the TEM images of the $AMoO_4$ nanoparticles synthesized with PHA:OAm = 1:0, 1:2, and 0:1. The diameters of the $CaMoO_4$, nanoparticles synthesized with PHA:OAm = 1:0, 1:2, and 0:1 are 58 ± 12, 33 ± 6, and 39 ± 5 nm, respectively. The diameters of the $BaMoO_4$, nanoparticles synthesized with PHA:OAm = 1:0, 1:2, and 0:1 are 326 ± 157, 48 ± 15, 453 ± 161 nm, respectively. The diameters of the $SrMoO_4$, nanoparticles synthesized with PHA:OAm = 1:0, 1:2, and 0:1 are 353 ± 91, 20 ± 6, 427 ± 122 nm, respectively. It was confirmed that the $SrMoO_4$ nanoparticles synthesized with PHA:OAm = 1:2 were the smallest in the all samples.

The particle size of $SrMoO_4$ is the smallest among the synthesized nanoparticles. One of the plausible reasons of the particle size differences is suppression of growth and aggregation causing to the lower surface energy of $SrMoO_4$ than those of others[21] and the effect of high density modification. It has been reported that the size of composite oxide nanoparticles depend on the surface energy.[22]

The small sizes of these nanoparticles are suitable for transparent dispersion in liquid scintillators because of the suppression of Mie scattering.

Figure 5 shows the photographic images of the nanoparticle dispersions in toluene (upper phase). The dispersions were stable overnight. The dispersions were irradiated with green laser light to observe Tyndall scattering; however, distinctive scattering was not observed. The Mo concentrations in the dispersions were determined using ICP-AES. **Table 3** summarizes the Mo concentration in $AMoO_4$ nanoparticle dispersions synthesized with PHA:OAm = 1:0, 1:2, and 0:1. The obtained values of the $AMoO_4$ nanoparticles synthesized with PHA:OAm = 1:2 were on the same order as that of the liquid scintillators comprising Mo as an organometallic complex or inorganic salts.

Figure 6 shows the TGA curves of the $AMoO_4$ nanoparticle-toluene dispersions synthesized with PHA:

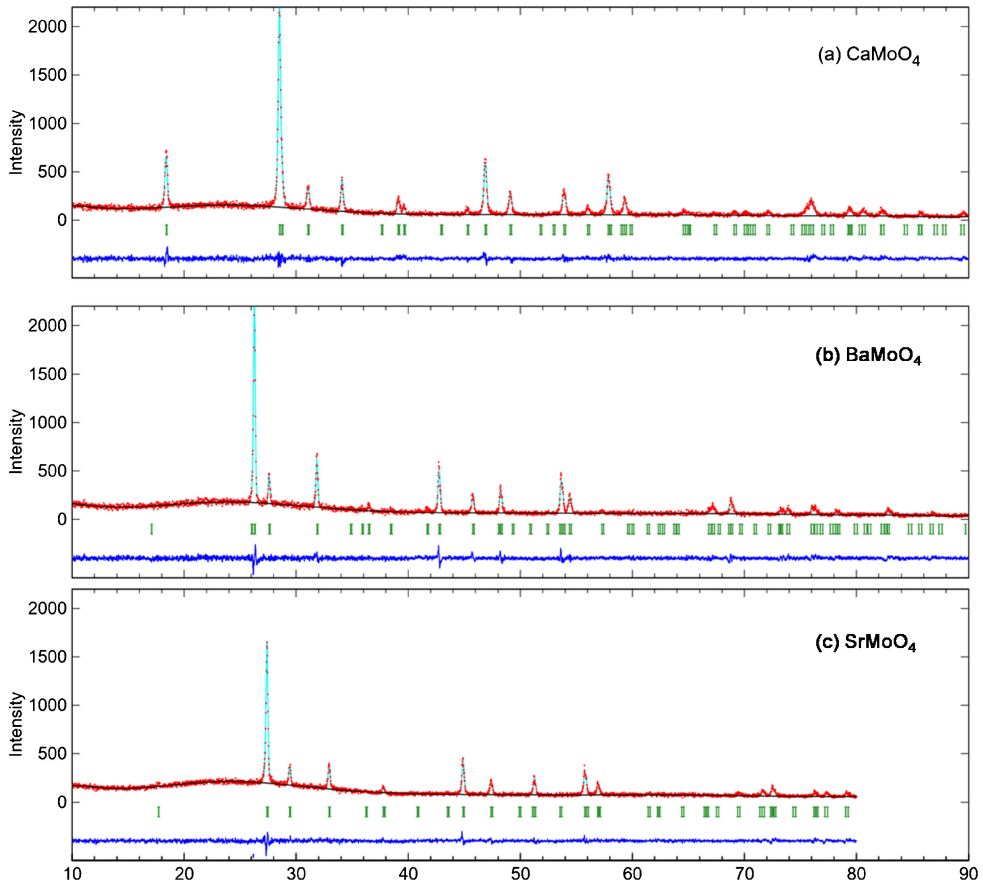

Fig. 3. XRD patterns of nanoparticles of (a) $CaMoO_4$, (b) $BaMoO_4$, and (c) $SrMoO_4$, synthesized with PHA:OAm = 1:2. Reliability factors of Rietveld fitting were (a) $CaMoO_4$, $R_{wp} = 13.52$, $S = 1.39$; (b) $BaMoO_4$, $R_{wp} = 13.87$, $S = 1.43$; and (c) $SrMoO_4$ $R_{wp} = 9.58$, $S = 1.07$.

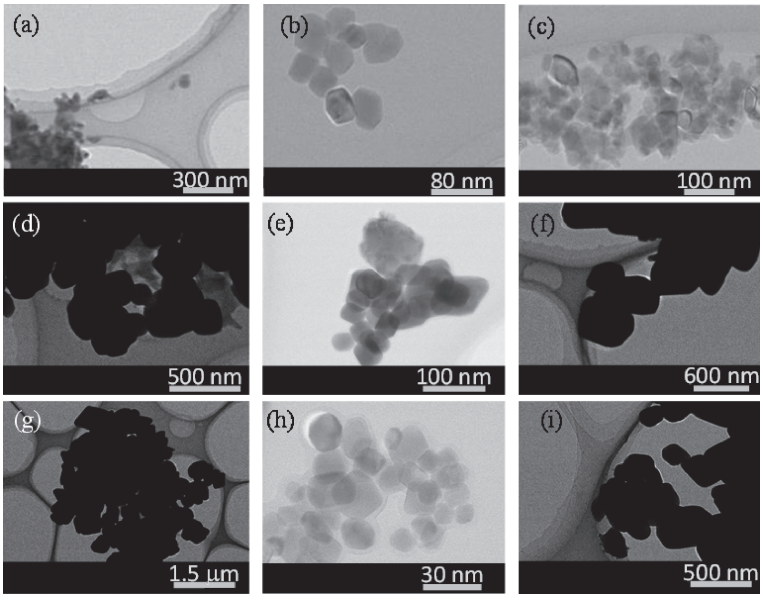

Fig. 4. TEM images of nanoparticles of $CaMoO_4$ nanoparticles synthesized in different molar ratios of PHA and OAm. (a) 1:0, (b) 1:2, (c) 0:1, $BaMoO_4$ nanoparticles synthesized in different molar ratios of PHA and OAm. (d) 1:0, (e) 1:2, (f) 0:1, and $SrMoO_4$ nanoparticles synthesized in different molar ratios of PHA and OAm. (g) 1:0, (h) 1:2, and (i) 0:1.

Table 3. Mo concentrations in $AMoO_4$ nanoparticle dispersions synthesized with PHA:OAm = 1:0, 1:2, and 0:1

	$CaMoO_4$			$BaMoO_4$			$SrMoO_4$		
PHA:OAm	1:0	1:2	0:1	1:0	1:2	0:1	1:0	2:1	0:1
Mo concentration [wt%]	0.082	0.43	0.12	0.071	0.21	0.027	0.00	0.054	0.040

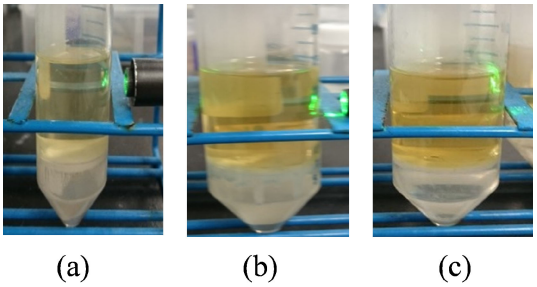

Fig. 5. Photographic images of nanoparticle-toluene dispersions of (a) $CaMoO_4$, (b) $BaMoO_4$, and (c) $SrMoO_4$, synthesized with PHA:OAm = 1:2. Mo concentration in these nanoparticle dispersion were 0.43, 0.21, and 0.054 wt%, respectively.

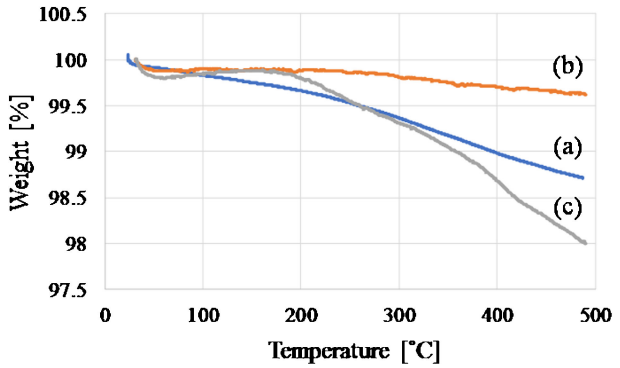

Fig. 6. TGA curves of nanoparticles of (a) $CaMoO_4$, (b) $BaMoO_4$, and (c) $SrMoO_4$, synthesized with PHA:OAm = 1:2.

OAm = 1:2. The weight loss values for $CaMoO_4$, $BaMoO_4$, and $SrMoO_4$ were 1.3, 0.4, and 1.8%, respectively. The surface modification density of the nanoparticles was estimated on the basis of the weight loss as 0.7, 0.6, and 0.5 chains/nm^2, respectively. The surface modification densities were lower than the typical values of well-modified nanoparticles, over 2.0 chains/nm^2. As for PHA and OAm at the surface of the nanoparticles, we estimated the ratios with CHNS analyzer. The ratios of PHA and OAm were 1:2.5, 1:1.6 and 1:1.5 for $CaMoO_4$, for $BaMoO_4$, and for $SrMoO_4$. It was confirmed that the $AMoO_4$ nanoparticles were modified by PHA and OAm.

Figure 7 shows the Mo 3d XPS spectrum of $SrMoO_4$. The peaks were observed at 235.2 and 232.2 eV and are attributed to Mo^{6+} $3d_{3/2}$ and $3d_{5/2}$.[23] The existence of Mo^{6+} in $SrMoO_4$ was proved.

Figure 8-A shows the absorption spectrum of the toluene dispersion of $SrMoO_4$ nanoparticles. The dispersion has a high transparency at wavelengths longer than 430 nm. The high optical density at short wavelengths can be attributed to the interband excitation of $SrMoO_4$, similar to the result reported in a previous paper.[24]

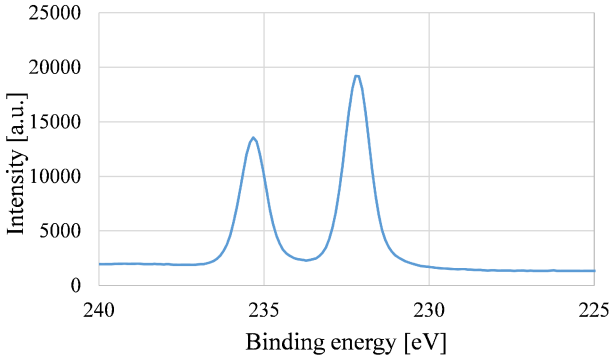

Fig. 7. Mo $3d_{3/2}$ and $3d_{5/2}$ XPS spectra of $SrMoO_4$ nanoparticles synthesized with PHA:OAm = 1:2.

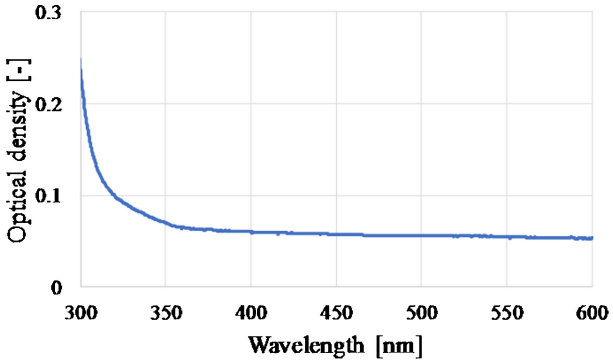

Fig. 8-A. Absorption spectrum of $SrMoO_4$ nanoparticle-toluene dispersion synthesized with PHA:OAm = 1:2.

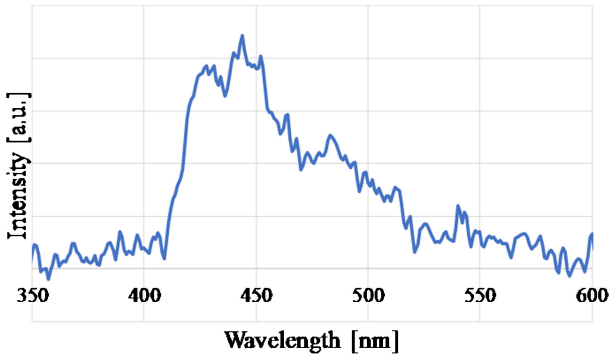

Fig. 8-B. X-ray-induced radioluminescence spectrum of the liquid scintillator incorporating $SrMoO_4$ nanoparticles synthesized with PHA:OAm = 1:2.

Figure 8-B depicts the X-ray-induced radioluminescence spectrum of the liquid scintillator incorporating $SrMoO_4$ nanoparticles. A dominant band is observed at 430 nm and is attributed to the emission from POPOP. Energy transfer from toluene to the luminescent material, POPOP, occurred successfully. A similar emission

wavelength is expected for beta-ray scintillation. Considering the absorption spectrum shown in Fig. 8-A, the liquid scintillator can be transparent at the scintillation wavelength.

4. Conclusions

For developing a liquid scintillator that contains a candidate isotope in high concentration and has high transparency, we focused ^{100}Mo as the candidate isotope and adopted organically modified nanoparticles, $AMoO_4$, synthesized with the subcritical hydrothermal method to disperse the isotope metal well in organic solvents. The size of $SrMoO_4$ nanoparticles synthesized with PHA:OAm = 1:2 was 20 ± 6 nm, the smallest among the synthesized nanoparticles samples. The liquid scintillator loaded with $SrMoO_4$ nanoparticles was transparent at scintillation wavelength longer than 430 nm, and the peak originated from phosphor emission was observed around 430 nm. Consequently, small organically modified $SrMoO_4$ nanoparticles, synthesized with subcritical hydrothermal syntheses, can be applied to liquid scintillators for neutrinoless double-beta decay experiments.

Acknowledgements This research was partially supported by a Grant-in-Aid for Young Scientists (A) (No. 25709088, 2013–2015) and a grant from The Sumitomo Foundation. This work was performed under the Research Program of "Dynamic Alliance for Open Innovation Bridging Human, Environment and Materials" in "Network Joint Research Center for Materials and Devices."

References

1) J. D. Vergados, H. Ejiri and F. Šimkovic, *Int. J. Mod. Phys. E*, 25, 1630007 (2016).
2) S. Dell'Oro, S. Marcocci, M. Viel and F. Vissani, *Adv. High Energy Phys.*, 37, 2162659 (2016).
3) C. Buck and M. Yeh, *J. Phys. G Nucl. Partic.*, 43, 093001 (2016).
4) I. B. Nemchenok, V. B. Brudanin, O. I. Kochetov, V. V. Timkin and A. A. Shurenkova, *Bull. Russ. Acad. Sci.: Phys.*, 75, 1007–1010 (2011).
5) M. J. Hwang, Y. J. Kwon, H. J. Kim, J. W. Kwak, S. C. Kim, S. K. Kim, T. Y. Kim, S. Y. Kim, H. S. Lee, M. J. Lee, S. S. Myung, Y. D. Kim, J. I. Lee, W. G. Kang, I. S. Hahn and M. H. Lee, *Astropart. Phys.*, 31, 412–416 (2009).
6) A. Meregaglia, J. Busto, C. Cerna, M. Chauveau, A. Dastgheibi-Fard, C. Jollet, S. Jullian, I. Katsioulas, I. Giomataris, M. Gros, P. Lautridou, C. Marquet, X. F. Navick, F. Perrot, F. Piquemal, L. Simard and M. Zampaolo, *JINST*, 13, P01009 (2018).
7) J. H. Arling, M. Gerhardt, C. Gößling, D. Gehre, R. Klingenberg, K. Kröninger, C. Nitsch, T. Quante, K. Rohatsch, J. Tebrügge, R. Temminghoff, R. Theinert, S. Zatschler and K. Zuber, *Phys. Ins. Det*, 12, 11025 (2017).
8) A. E. Chavarria, C. Galbiati, X. Li and J. A. Rowlands, *JINST*, 12, P03022 (2017).
9) S. Takami, S. Ohara, T. Adschiri, Y. Wakayama and T. Chikyow, *Dalton T.*, 40, 5442–5446 (2008).
10) T. Adschiri, K. Kanazawa and K. Arai, *J. Am. Ceram. Soc.*, 75, 1019–1022 (1992).
11) T. Adschiri, *Chem. Lett.*, 36, 1188–1193 (2007).
12) T. Adschiri and A. Yoko, *J. Supercrit. Fluids*, 134, 167–175 (2018).
13) S. Takigawa, M. Koshimizu, T. Noguchi, T. Aida, S. Takami, T. Adschiri, A. Yoko, G. Seong, Y. Fujimoto and K. Asai, *J. Radioanal. Nucl. Ch.*, 314, 611–615 (2017).
14) Z. Xian-Ju, C. Jia and Y. Xiao-Dong, *Chin. J. Inorg. Chem.*, 28, 932–936 (2012).
15) M. Watanabe, M. Osada, H. Inomata, K. Arai and A. Kuruse, *Appl. Catal. A-Gen.*, 245, 333–341 (2003).
16) N. C. Halder and C. N. J. Wagner, *Acta Crystallogr.*, 20, 312–313 (1966).
17) F. Izumi and K. Momma, *Solid State Phenom.*, 130, 15–20 (2007).
18) T. Ida and H. Toraya, *Funtai Kogaku Kaishi*, 40, 177–184 (2003).
19) T. D. Nguyen, C. T. Dinh, D. T. Nguyen and T. O. Do, *J. Phys. Chem. C*, 113, 18584–18595 (2009).
20) W. Bu, Z. Chen, F. Chen and J. Shi, *J. Phys. Chem. C*, 113, 12176–12185 (2009).
21) A. P. A. Marques, M. T. S. Tanaka, E. Longo, E. R. Leite and I. L. V. Rosa, *J. Fluoresc.*, 21, 893–899 (2011).
22) A. Yoko, N. Umezawa, T. Ohno and Y. Oshima, *J. Phys. Chem. C*, doi:10.1021/acs.jpcc.8b06149.
23) J. G. Choi and L. T. Thompson, *Appl. Surf. Sci.*, 93, 143–149 (1996).
24) T. Thongtema, S. Kungwankunakorna, B. Kuntalueb, A. Phuruangratc and S. Thongtem, *J. Alloy. Compd.*, 506, 475–481 (2010).